Supplementary Information

Integrating Singlet Oxygen–Driven Photocatalytic H_2O_2 Synthesis with Uranium(VI) Sequestration by a Pyrene-Based Porous Aromatic Framework

Flora Banerjee,[a] Swarnava Bhattacharyya,[†,a] Tanushree Nath,[†,a] Shubhangi Majumdar,[†,b] Koushik Mitra,[c] Samarpita Das,[d] Pramit K. Chowdhury,[b] and Suman Kalyan Samanta* [a]

Department of Chemistry, Indian Institute of Technology Kharagpur, Kharagpur 721302, India. E-mail: sksamanta@chem.iitkgp.ac.in

Department of Chemistry, Indian Institute of Technology Delhi. Delhi, Hauz Khas, New Delhi-110016, India.

Department of Industrial Chemistry & Applied Chemistry, Swami Vivekananda Research Centre, Ramakrishna Mission Vidyamandira, Belur Math, Howrah 711202, India.

Department of Chemistry, Indian Institute of Engineering Science and Technology, Howrah 711 103, West Bengal, India.

1. Experimental Section

1.1. Materials and Methods. All the reagents, starting materials (1,3,6,8-tetrabromopyrene, anhy. $FeCl_3$, 4-bromo-2-naphthol), solvents and catalysts were purchased from commercial suppliers and were used without further purification. Solvents were dried as per literature procedure prior to use according to the requirements. Thin layer chromatography (TLC) on silica gel GF_{254} was used for the determination of R_f values, and the visualization was performed by irradiation with UV lamp at 254 nm. Column chromatography was performed on Merck silica gel (100-200 mesh) with eluent as mentioned. ^1H (500 MHz) and ^{13}C (125 MHz) NMR spectra were recorded in a Bruker advance-500 NMR spectrometer in deuterated solvent at ambient temperature (300 K). Chemical shifts are reported in ppm (δ) relative to tetramethylsilane (TMS) as the internal standard ($CDCl_3$ δ 7.26 ppm for ^1H and 77.0 ppm for ^{13}C; DMSO-d_6 δ 2.5 and 3.6 ppm for ^1H and 39.26 ppm for ^{13}C). Solid state ^{13}C CPMAS NMR spectra were recorded in a Bruker Ultrashield-500 NMR spectrometer. Mass spectra were recorded on Agilent 6500 Series Q-TOF spectrometer. MALDI-ToF spectra were acquired with BRUKER Ultraflextreme spectrometer. Fourier transform infrared spectra (FTIR, 4000-600 cm^{-1}) were performed on Nicolet 6700 FT-IR spectrometer (Thermo Fischer) instrument, the wave numbers of recorded IR-signals are reported in cm^{-1}. Elemental analyses were carried out using a Perkin-Elmer Series-II, CHN/S Analyser-2400. Thermogravimetric analyses (TGA) were performed on a Pyris Diamond Tg Dta (PerkinElmer) instrument. The BINOL based porous organic polymers were observed under scanning electron microscope (SEM) model ZEISS SUPRA 40. The samples were prepared on aluminum stubs by adding powder polymers mounting on top of double-sided tapes. HRTEM measurements were carried out in a JEOL-JEM-F200 machine operating at an accelerating voltage of 200 V. TEM samples were prepared by mounting on the copper grid for analysis. UV-visible adsorption spectra were recorded on a Shimadzu UV-2550 UV-vis spectrophotometer. X-Ray diffraction patterns of the powder organic polymer samples were obtained using a Bruker AXS D-8Advanced SWAX diffractometer using Cu-Kα (0.15406 nm) radiation. The N_2 adsorption/desorption isotherms of the sample was recorded on a Micromeritics 3-Flex Surface Characterization Analyzer at 77 K.

1.2. Synthesis of Monomer 2. A mixture of 1,3,6,8-tetrabromopyrene (140 mg, 0.26 mmol, 1 equivalent), compound **1** (435 mg, 1.6 mmol, 6 equivalents), Na_2CO_3 (275 mg, 10 equivalents), and $[Pd(PPh_3)_4]$ (5 mol%, 15 mg) was dissolved in 12 mL of a dioxane/H_2O solvent mixture (3:1). The reaction was stirred under an argon atmosphere at 90 °C for five days. Upon completion, the mixture was cooled to room temperature, treated with water, and extracted with ethyl acetate. The organic layer was washed with brine, dried over Na_2SO_4, and concentrated under reduced pressure. The crude product was purified by column chromatography on silica gel using a chloroform/methanol solvent system (20:1), yielding a brown solid with a 70% yield. ^1H NMR (500 MHz, DMSO-d_6, ppm): 9.90 (4H, s); 7.98 (2H, d); 7.80-7.82 (4H, m); 7.58-7.61 (4H, t); 7.40 (2H, t); 7.36 (2H, s); 7.26-7.31 (12H, m); 7.11-7.16(4H, m).^{13}C NMR (125 MHz, DMSO-d_6, ppm): 155.02, 139.46, 135.80, 135.39, 130.78, 129.53, 127.67, 127.16, 126.69, 126.15, 126.01, 124.91, 123.56, 121.31, 109.72. FT-IR (KBr pellet, cm^{-1}): 3323, 2974, 1548, 1189, 789. MALDI-TOF: 770.2500 (Calculated); 770.1190 (Observed).

1.3. Synthesis of Pyrene-BINOL-4. The monomer **2** (86 mg, 1 equiv.) was dissolved in dichloroethane in the presence of anhydrous $FeCl_3$ (126 mg, 7 equiv.) and refluxed for 5 days.

Afterwards, the resultant precipitate was filtered and subjected to multiple washings with HCl and MeOH. Subsequently, the precipitate underwent Soxhlet extraction for 48 hours with $CHCl_3$, acetone, and MeOH. Finally, it was dried under vacuum, yielding a brown polymer with 79% yield. IR (KBr pellets, cm^{-1}): 3419, 2932, 1548, 1172,761. ^{13}C NMR (CP/MAS solid state, ppm): 156, 143, 135, 120-132, 116, 110. Fe content: 0.077 wt.% (ICP-MS) and Cl content: 0.001 wt.% (IC). TGA: 5% wt. loss at 365 °C.

1.4. Calculation for VB XPS:

The results obtained for valence band offset (VB_{xps}) of **Pyrene-BINOL-4** is 1.38 eV. The electron work function (Φ) of the analyzer was 4.35 eV. Using these values in equation 1, the valence band potential could be obtained

$E_{VB} = \Phi + VB_{xps} - 4.44$ …….(S1)

The E_g value, i.e., optical band gap, was calculated from the Tauc plot.

$E_{CB} = E_{VB} - E_g$…….(S2)

1.5. Procedure for quantification of H_2O_2:

A Pyrex tube was charged with solid photocatalyst (2 mg) in water (5 mL) without or with a sacrificial reagent (MeOH) (0.5 mL) (water: SA = 10:1), and then ultrasonicated for 10-15 min (to disperse the POP) after being capped under air. For an oxygen atmosphere, the flask was purged with O_2 for 15 minutes in each case. The temperature was maintained by circulating cold water. Then, it was irradiated for an hour under a 50 W blue LED. The amount of H_2O_2 was analyzed by titration using ceric sulfate (0.1 M) with ferroin as an indicator.

$$H_2O_2(wt.\%) = \frac{Volume\ of\ Ce(SO_4)_2\ (L) \times 0.1 mol\ L^{-1} \times 0.5\ \frac{mole\ H_2O_2}{mole\ \ Ce(SO_4)_2} \times \frac{34.01\ g\ H_2O_2}{mol\ H_2O_2}}{Weight\ of\ sample\ (g)} \ldots (S3)$$

1.6. EIS data:

The Nyquist plot was obtained using the electrochemical impedance spectroscopy (EIS) technique, measured within the 100-1000 Hz frequency range at E= 0 $V_{Ag/AgCl}$ using DC voltage with an introduction of 5 mV under illuminated conditions.

1.7. Photocurrent:

The transient photocurrent measurements were taken with CHI6600C instrument. photo-switching activity, i.e., current density versus time (j–t) plots of the polymer thin film on FTO substrate at 0.5 $V_{Ag/AgCl}$ in aq. 0.5M Na_2SO_4 solution. The system was purged with O_2 prior to the measurements.

1.8. Steady-state PL spectra:

The room temperature photoluminescence spectra were recorded with a FLSP-980 spectrofluorometer (Edinburgh), having a Xe lamp source with an excitation wavelength of 400 nm.

1.9. Transient Absorption Spectra:

Ultrafast transient absorption measurements were conducted using a commercial one-box ultrafast Ti: Sapphire amplifier (Astrella 1K-F, 100 fs, 5 mJ/pulse, and 1 kHz repetition rate, Coherent Inc.,) with an integrated oscillator (Vitara-S, 400 mW at 800 nm, 70 nm bandwidth, pumped by Verdi-G, 80 MHz) and coupled to a femtosecond transient absorption spectrometer (Helios Fire UV-VIS, Ultrafast Systems). The amplified output (5mJ/pulse, 1 kHz) of central wavelength 800 nm was divided into two parts. One part (~200 mW) was used to produce the femtosecond probe pulse by focusing it either on a CaF_2 (for UV probe: 310 – 615 nm) or 2-mm thick sapphire crystal for white light continuum (400-800 nm) while the other part (3.25 mW) was used to generate a tunable femtosecond pump pulse using an optical parametric amplifier (OPerA Solo, 290 – 2600 nm). After the sample, the probe beam (1 kHz) was collimated and then focused into a fiber-optics coupled multichannel spectrometer equipped with CMOS sensor (1024 pixels). The pump power used in the experiment was controlled by a variable neutral-density filter wheel and kept at ~0.5 mW. Both the pump and probe beams overlapped at the sample cuvette and the delay between the pump and probe pulses was controlled by a motorized delay stage. The pump pulses were chopped by a synchronized chopper at 500 Hz and the absorbance change was calculated with two adjacent probe pulses (pump-blocked and pump-unblocked).

Calculations of Decay Time:

The transient decays were fitted by equation (S4), using an IRF of ~150 fs with the help of Surface Xplorer software and the average lifetimes were calculated according to equation (S5). $\Delta A\ (\lambda, t)$ is the observed change in absorbance at time t and wavelength λ, A is the amplitude and τ is the time constant of i^{th} component.

$$\Delta A\ (\lambda, t) = A_0 + \sum_i A_i\, e^{-\frac{t}{\tau_i}} \qquad \text{(S4)}$$

$$< \tau >= \frac{\sum_i A_i \tau_i}{\sum_i A_i} \qquad \text{(S5)}$$

1.10. Rotating Disc Electrode:

The electron transfer number for the oxygen reduction reaction was measured on a rotating disk electrode (RDE) in O_2-saturated 0.5 M Na_2SO_4 (pH = 7) solution at room temperature with different rotating speeds (rpm) (after O_2 bubbling for 40 min. The number of electron transfer can be calculated by the following Koutecky-Levich equation.

$$\frac{1}{J} = \frac{1}{JL} + \frac{1}{JK} = \frac{1}{B\sqrt{\omega}} + \frac{1}{JK} \qquad \text{(S6)}$$

$$B = 0.2\text{nF}V^{-\frac{1}{6}}\text{C}D^{\frac{2}{3}} \qquad \text{(S7)}$$

Where J is the current intensity, J_L and J_K are the kinetic and diffusion-limiting current densities, ω is the angular velocity, n is the transferred electron number, F is Faraday constant (96485 C mol^{-1}), *V* is the kinetic viscosity of water (0.01 cm^2 s^{-1}), C is the bulk concentration of O_2 in water (1.26×10^{-3} mol cm^{-3}), and D is the diffusion coefficient of O_2 (2.7×10^{-5} cm^2 s^{-1}).

The RRDE measurements were carried out using a standard three-electrode configuration on a CHI760E electrochemical workstation equipped with an RRDE-3A system, where a glassy carbon disk (coated with the photocatalyst) and a Pt ring served as the working electrode, along with a Ag/AgCl (saturated KCl) reference electrode and a Pt wire counter electrode. The catalyst ink was prepared by dispersing the photocatalyst in a mixture of water/isopropanol with a small amount of Nafion binder, followed by sonication and drop-casting onto the disk surface. The electrochemical measurements were performed in an O_2-saturated electrolyte 0.1 M Na_2SO_4, achieved by bubbling high-purity oxygen for at least 20 minutes prior to measurement and maintaining a gentle O_2 flow throughout the experiment. Linear sweep voltammetry was conducted at a slow scan rate (10 mV s^{-1}) with rotation speed (400 rpm), while the ring electrode was held at a constant potential of approximately +0.7 V vs Ag/AgCl to selectively oxidize the H_2O_2 generated at the disk. The disk and ring currents were simultaneously recorded, enabling calculation of the electron transfer number and H_2O_2 selectivity based on the collection efficiency of the ring electrode (N = 0.43).

1.11. Solar to Chemical conversion efficiency:

$$SCC\ efficiency\ \% = \frac{[\Delta G\ for\ H_2O_2\ production\ (Jmol^{-1})][H_2O_2\ formed\ (mol)]}{[Total\ input\ power\ (W)][Reaction\ time\ (s)]} \times 100 \ldots \text{(S8)}$$

The SCC efficiency was calculated with the help of an AM 1.5G solar simulator, with H_2O_2 produced 0.000382 mol. The free energy change is 117 kJ.mol^{-1}. The irradiation cross-sectional area was 13.28 cm^2. Light intensity was 100 mW/cm^2.

1.12. Procedure for estimation of apparent Quantum Yield:

The apparent quantum yield (AQY) was determined under LED light irradiation (with band filter) at a certain wavelength (λ = 456 nm), and the light intensity was measured by a PM100D Power with a photodiode sensor. The AQY was calculated using the following equation:

$$AQY\ \% = \frac{[H_2O_2\ produced\ (mol)] \times 2}{Photon\ number\ entered\ into\ the\ reactor\ (mol)} \times 100 \ldots \text{(S9)}$$

$$= \left[[Na \times h \times c] \times\ [H_2O_2\ produced\ (mol)] \times 2\ \times 100\right] \div [I \times S \times t \times\times \lambda]$$

Where, Na is Avogadro's constant (6.022×10^{23} mol^{-1}), h is the Planck constant (6.626×10^{-34} J s), c is the speed of light (3×10^{8} m s^{-1}), S is the irradiation area (cm^2), I is the intensity of irradiation light ($W.cm^{-2}$), t is the photoreaction time (s), λ is the wavelength of the monochromatic light (m).

1.13. Computational study:

The geometry of all the model compounds were optimized with Gaussview 6.0 package and GAUSSIAN 16 software. The oxygen binding energies were calculated using DFT/B3LYP/6-31G* basis set.

time dependent density functional theory (TDDFT) within the Gaussian 16 program.[S1] The geometry optimizations, transition state calculations were done using B3LYP [S2-S3] functional with the basis set 6-31++g(d,p). The TD-DFT calculations for the excited states were conducted using the CAM-B3LYP [S4] functional, comprising long range corrections with the same basis set. For both the DFT and TDDFT calculations, Grimme's dispersion model D3 [S5] was employed to consider the non-covalent interaction. To ensure consistency with the experimental conditions, we considered a self-consistent reaction field (SCRF) model utilizing the SMD[S6] approach. The experimental solvent consisted of water actively participating in the reaction. Considering the dielectric constants of water (78.54)[S7], water was selected as a solvent Natural bonding orbital analysis (NBO) was conducted using the built-in NBO 3.1[S8] module within Gaussian 16.

1.14. EPR study:

Bruker ELEXSYS 580 spectrometer was used to record the EPR spectra. The specific measurement details regarding reactive oxygen species (ROS) trapping are as follows: the modulation frequency = 100.00 kHz, modulation amplitude = 3.000 G. The samples were prepared by adding 1 mg of photocatalyst to a 1 mL 0.1 M air-saturated THF/water solution of 2,2,6,6-Tetramethylpiperidine (TEMP).

1.15. General procedure for photoimmobilization of uranium(VI)

The photoimmobilization of U(VI) was carried out in a 25 mL quartz tube, the light source was a 50 W blue LED lamp. 1.5 mg photocatalyst **Pyrene-BINOL-4** was added into 5 mL U(VI) solution after achieving adsorption-desorption equilibrium was put for sonication. After irradiation, arsennazo III was used to analyse U(VI) concentration by UV–vis spectroscopy at the wavelength of 652 nm. Furthermore, the influences of pH, initial U(VI) concentration and coexisting interference ions on the photocatalytic U(VI) reduction performance were also investigated. The measured residual concentration of uranium with irradiation time can be converted into the photoreduction efficiency of uranium according to the following formula:

$$\mathbf{R_e = (C_0 - C_t)/C_0 \times 100\%} \quad \text{……(S10)}$$

where R_e is the reduction efficiency of uranium, C_0 is the initial concentration of uranium (ppm or mg L^{-1}), C_t is the uranium concentration at time (t) (ppm or mg/L).

The maximum extraction capacity was determined by the equation :

$$\mathbf{Q_m = (C_0 - C_e) \times V/m} \quad \ldots\ldots(S11)$$

V is the volume of solution in mL; m is the mass of polymer and C_e is the equilibrium concentration of UO_2^{2+} within solution. For recycling, the reacted suspension was centrifuged to remove the supernatant. The photocatalyst was then recovered by immersing it in 1 M HNO_3 and stirring vigorously to facilitate demetallization.

Seawater specifications: The salinity, Cl^- concentration, and turbidity of the seawater used in the present study from the coast of the Bay of Bengal (21.6222° N, 87.5066° E) suggest the following values- Salinity – 20.26 PSU (mean); Turbidity – 7.56 NTU (mean); Chloride concentration – 0.54 M. After achieving adsorption-desorption equilibrium, the residual uranium was subjected to photocatalytic removal under oxygen.

2. Characterizations

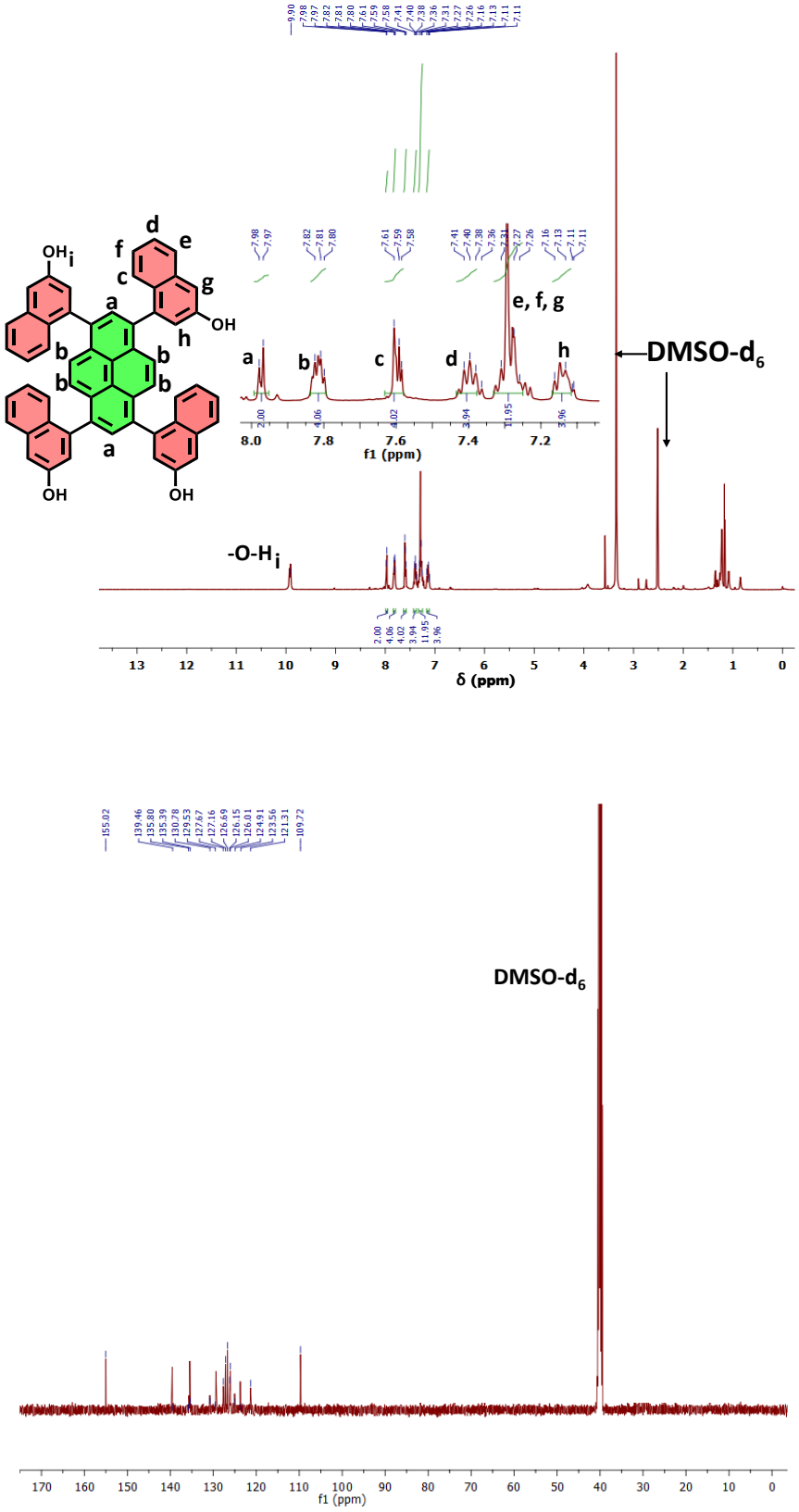

Figure S1. ^{1}H NMR and ^{13}C NMR of monomer **1** in DMSO-d_6

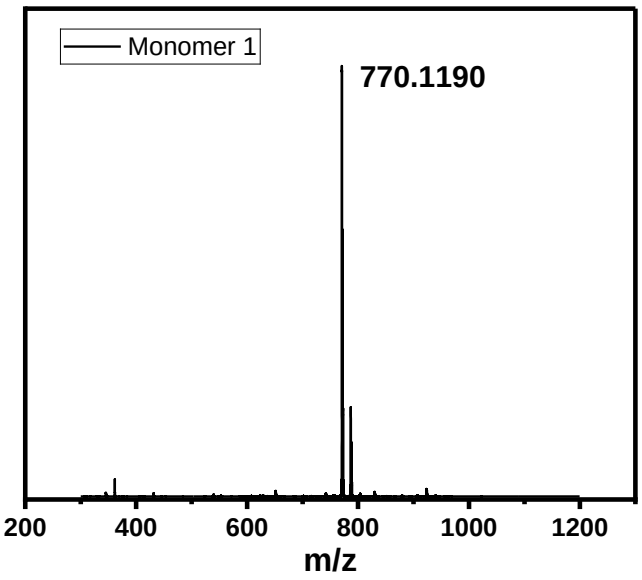

Figure S2. MALDI-Tof spectrum of monomer **1** (m/z calc. = 770.2500).

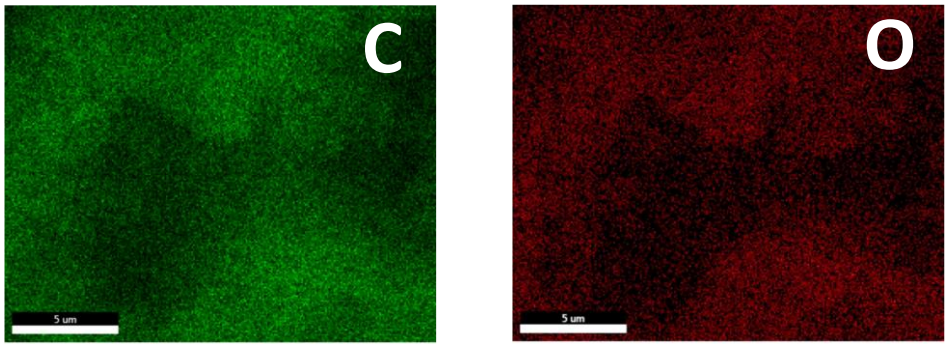

Figure S3. EDX elemental mapping of PAF **Pyrene-BINOL-4**

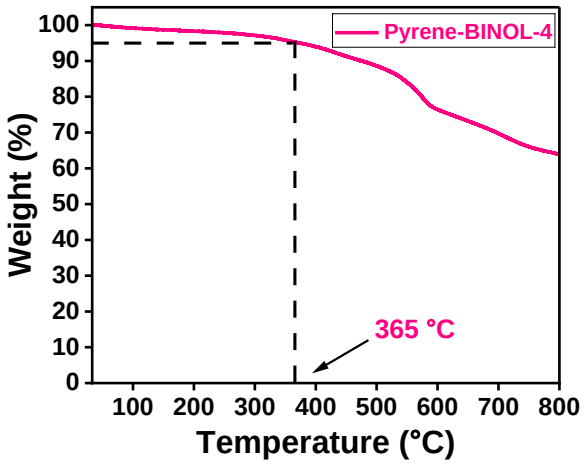

Figure S4. Thermogravimetric analysis of **Pyrene-BINOL-4** under nitrogen atmosphere.

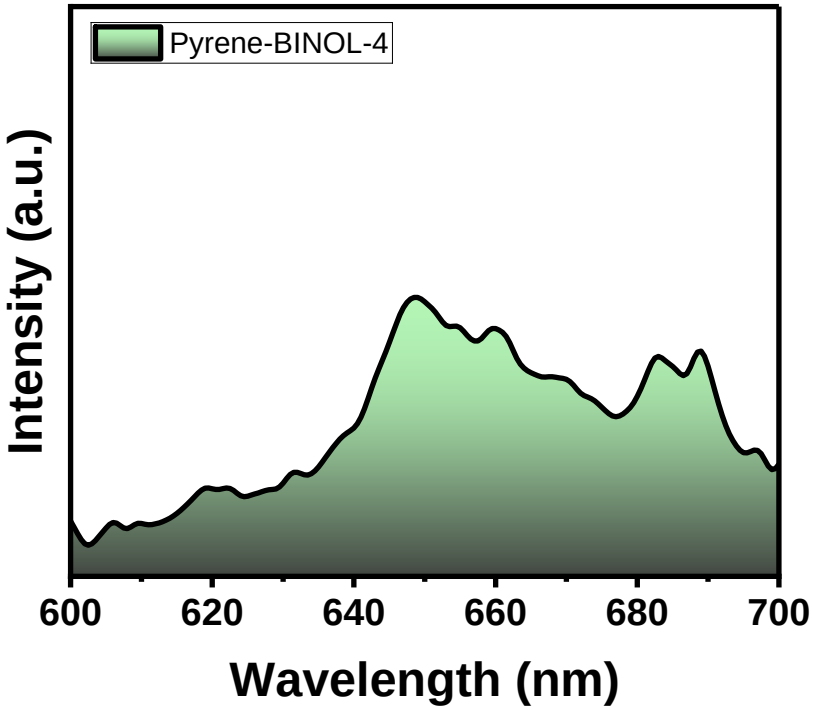

Figure S5. Solid-state photoluminescence spectrum of **Pyrene-BINOL-4**.

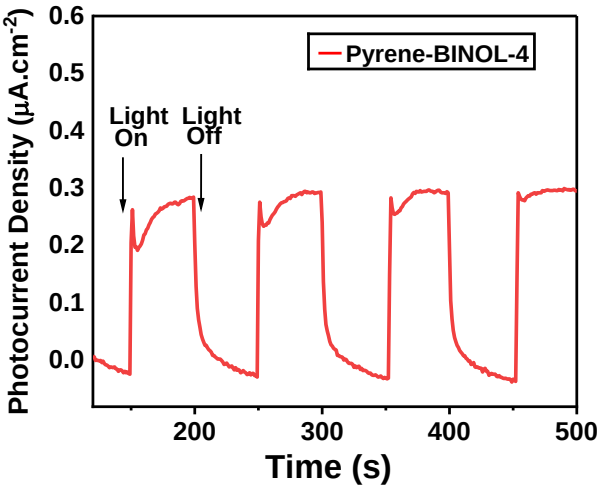

Figure S6. Transient photocurrent response of **Pyrene-BINOL-4** under 300 W Xe lamp**.**

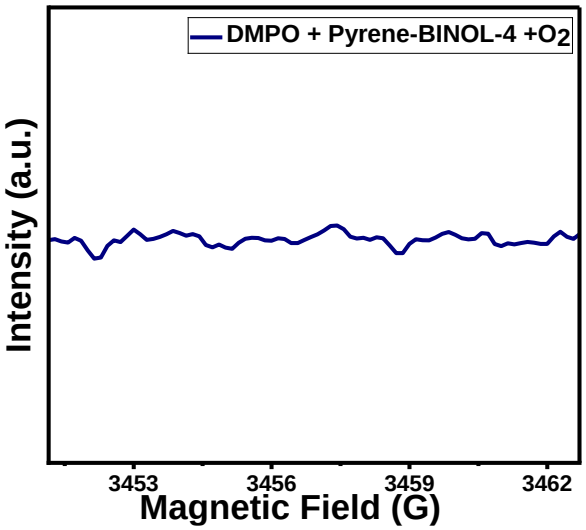

Figure S7. EPR spectra of **Pyrene-BINOL-4** in presence of DMPO after irradiation.

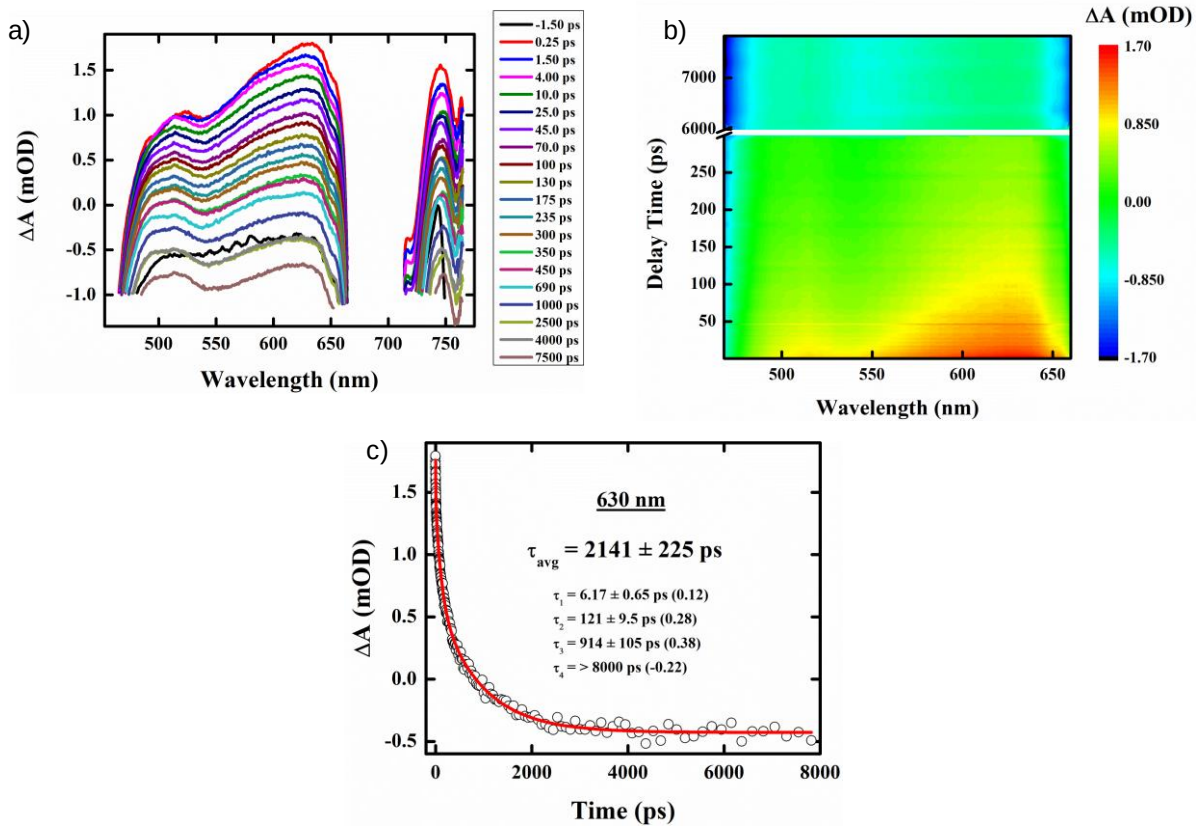

Figure S8. a) Time-dependent fs-TAS profile; b) 2D mapped contour fs-TAS spectra. c) Kinetic decay fitting plot for **Pyrene-BINOL-4** under nitrogen atmosphere**.**

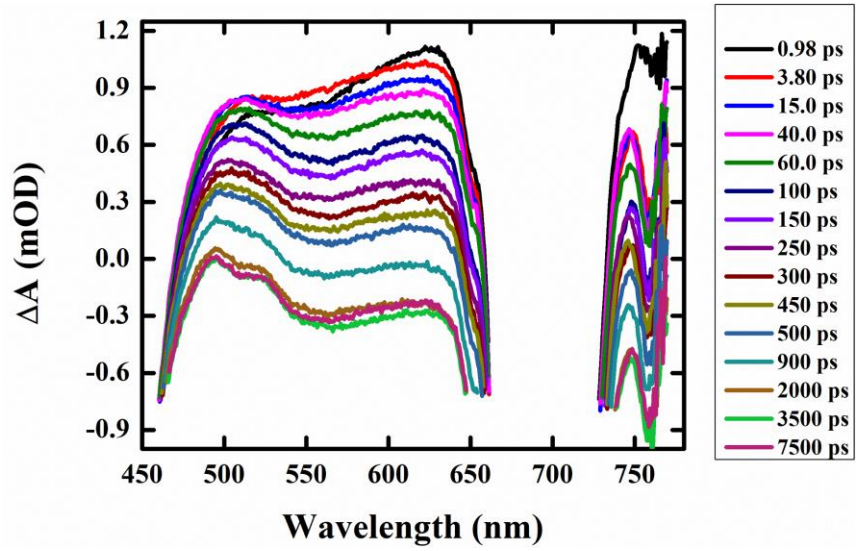

Figure S9. Time-dependent transient absorption profile for **Pyrene-BINOL-4** under an oxygen atmosphere.

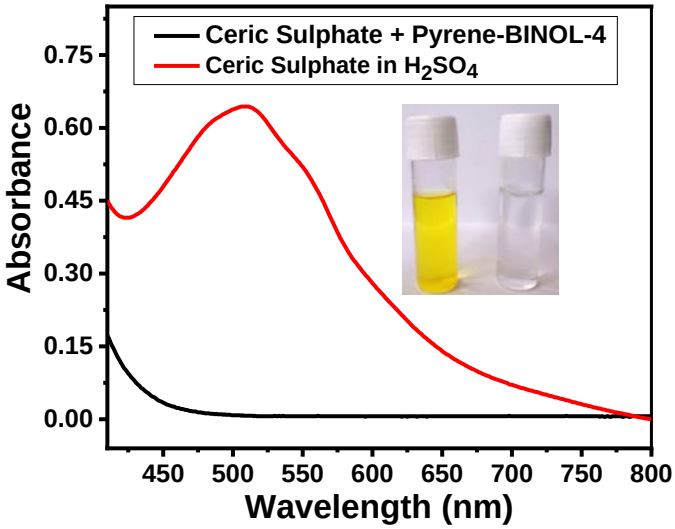

Figure S10. Qualitative analysis of H_2O_2 production with **Pyrene-BINOL-4** using ceric sulphate.

GC-MS Chromatogram.

(a)

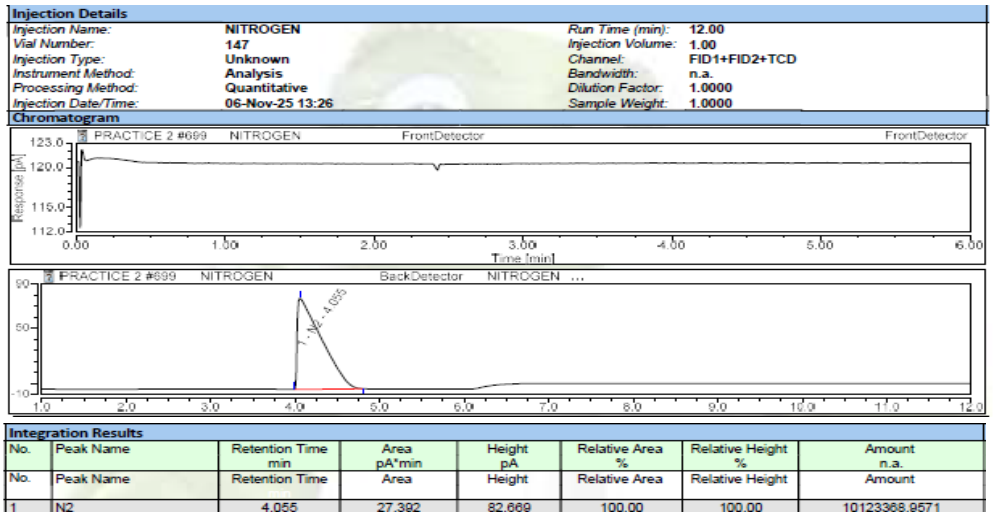

Injection Details			
Injection Name:	NITROGEN	Run Time (min):	12.00
Vial Number:	147	Injection Volume:	1.00
Injection Type:	Unknown	Channel:	FID1+FID2+TCD
Instrument Method:	Analysis	Bandwidth:	n.a.
Processing Method:	Quantitative	Dilution Factor:	1.0000
Injection Date/Time:	06-Nov-25 13:26	Sample Weight:	1.0000

Chromatogram

Integration Results

No.	Peak Name	Retention Time min	Area pA*min	Height pA	Relative Area %	Relative Height %	Amount n.a.
No.	Peak Name	Retention Time	Area	Height	Relative Area	Relative Height	Amount
1	N2	4.055	27.392	82.669	100.00	100.00	10123368.9571

(b)

Injection Details			
Injection Name:	PY4-45 MINS	Run Time (min):	12.00
Vial Number:	148	Injection Volume:	1.00
Injection Type:	Unknown	Channel:	FID1+FID2+TCD
Instrument Method:	Analysis	Bandwidth:	n.a.
Processing Method:	Quantitative	Dilution Factor:	1.0000
Injection Date/Time:	06-Nov-25 14:39	Sample Weight:	1.0000

Chromatogram

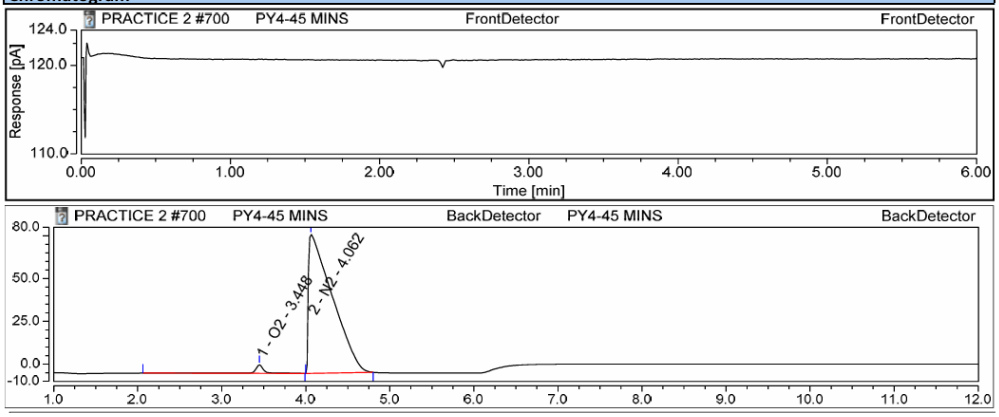

Integration Results

No.	Peak Name	Retention Time min	Area pA*min	Height pA	Relative Area %	Relative Height %	Amount n.a.
1	O2	3.448	0.704	4.983	2.58	5.78	19457.8058
2	N2	4.062	26.559	81.213	97.42	94.22	989734.6700

(c)

Injection Details

Injection Name:	**PY4-1HR50MIN**	*Run Time (min):*	**12.00**
Vial Number:	**149**	*Injection Volume:*	**1.00**
Injection Type:	**Unknown**	*Channel:*	**FID1+FID2+TCD**
Instrument Method:	**Analysis**	*Bandwidth:*	**n.a.**
Processing Method:	**Quantitative**	*Dilution Factor:*	**1.0000**
Injection Date/Time:	**06-Nov-25 15:42**	*Sample Weight:*	**1.0000**

Chromatogram

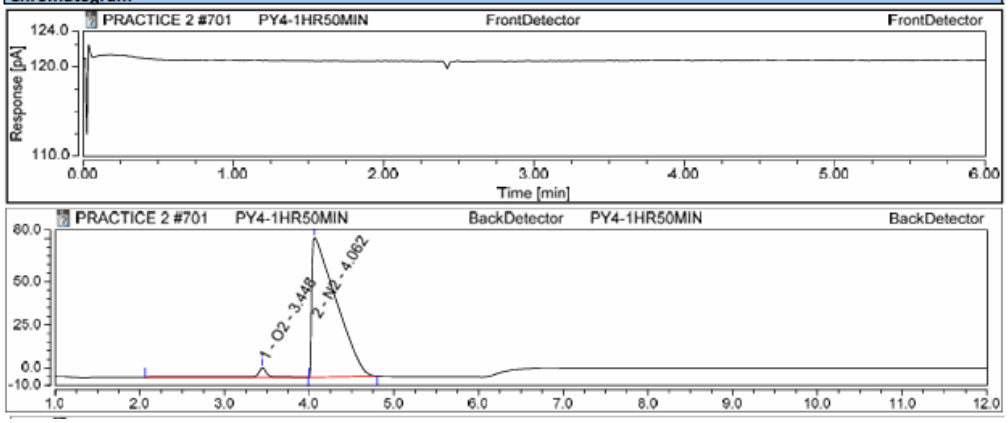

Integration Results

No.	Peak Name	Retention Time min	Area pA*min	Height pA	Relative Area %	Relative Height %	Amount n.a.
1	O2	3.448	0.750	5.525	2.75	6.37	20742.7296
2	N2	4.062	26.540	81.190	97.25	93.63	989049.3628

Figure S11. GC-MS profile of gas collected from headspace of aqueous dispersion of **Pyrene-BINOL-4** (0.5 mg/mL) under AM 1.5G simulator (with N_2-presaturation) ; (a) initially ; after (b) 45 min and (c) 1 h 50 min.

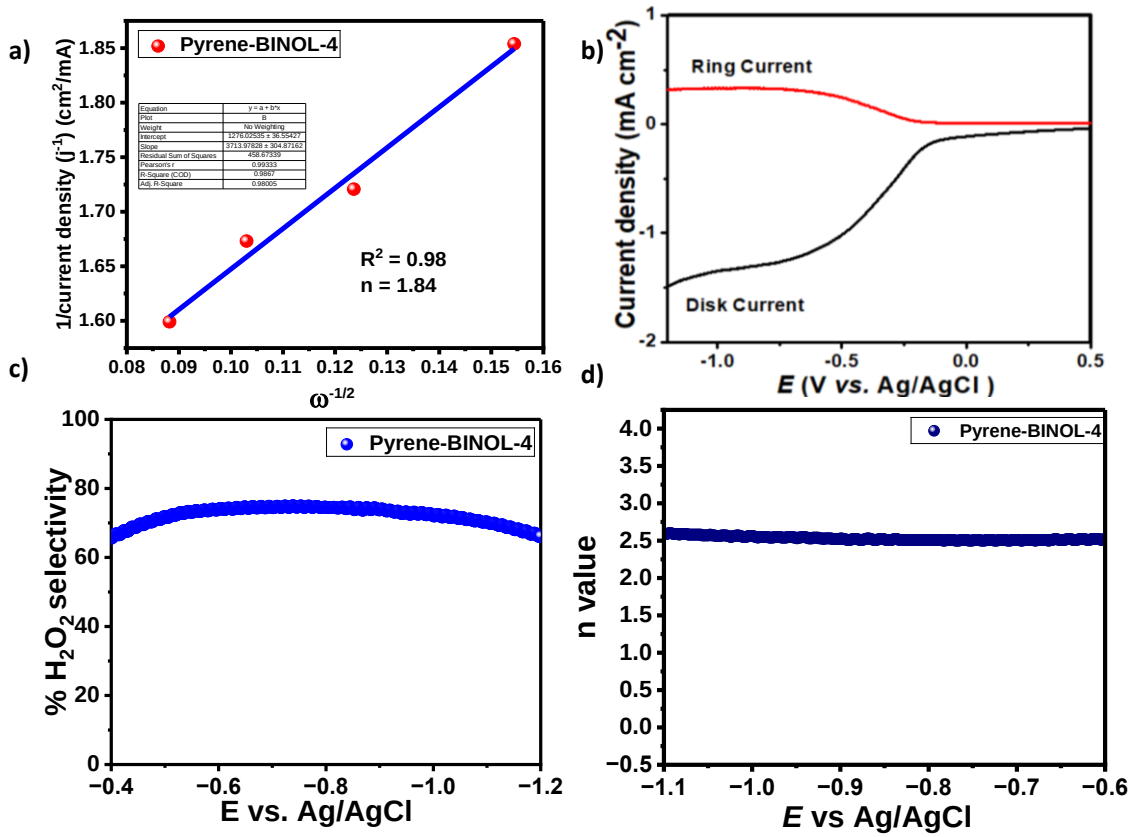

Figure S12. a) Koutecky-Levich plot for **Pyrene-BINOL-4** under oxygen; b) RRDE profile for **Pyrene-BINOL-4**; c) H_2O_2 selectivity under potential ranges; d) The average electron transfer under potential ranges.

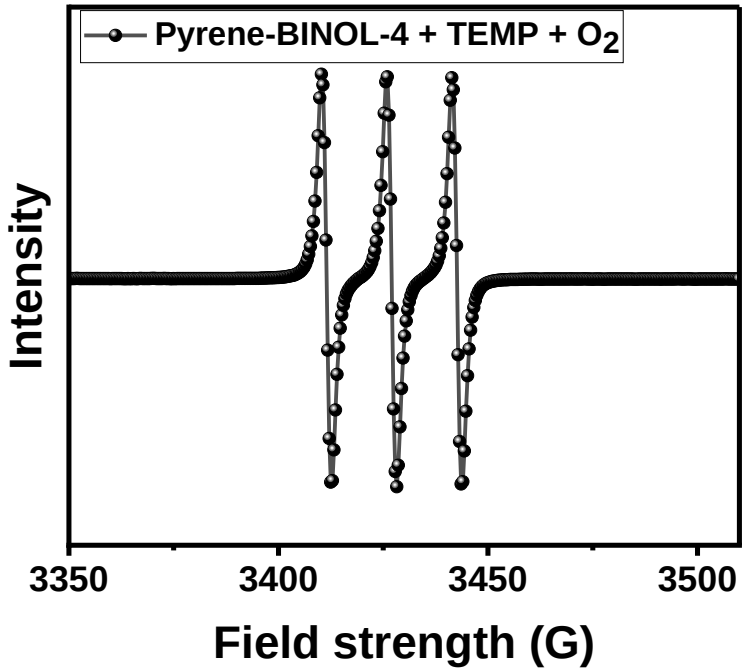

Figure S13. EPR spectrum of **Pyrene-BINOL-4** under oxygen in the presence of TEMP.

Table S1. The transition parameters for **Pyrene-BINOL-4** as determined with TDDFT calculations performed using water as solvent.

Transition	Excitation Energy(eV)	Wavelength (nm)	Oscillator Strength *(f)*
H-> L	2.68 (S_1)	461.17	0.7019
H-5 ->L H-3 -> L	3.05 (S_2)	405	0.1746
H -> L +1 H-6 -> L +8	2.55 (T_3)	486.27	0.0827
H-> L	1.83 (T_1)	635.27	0.6572
H -1 -> L H -> L +2	2.53 (T_2)	489.13	0.2341

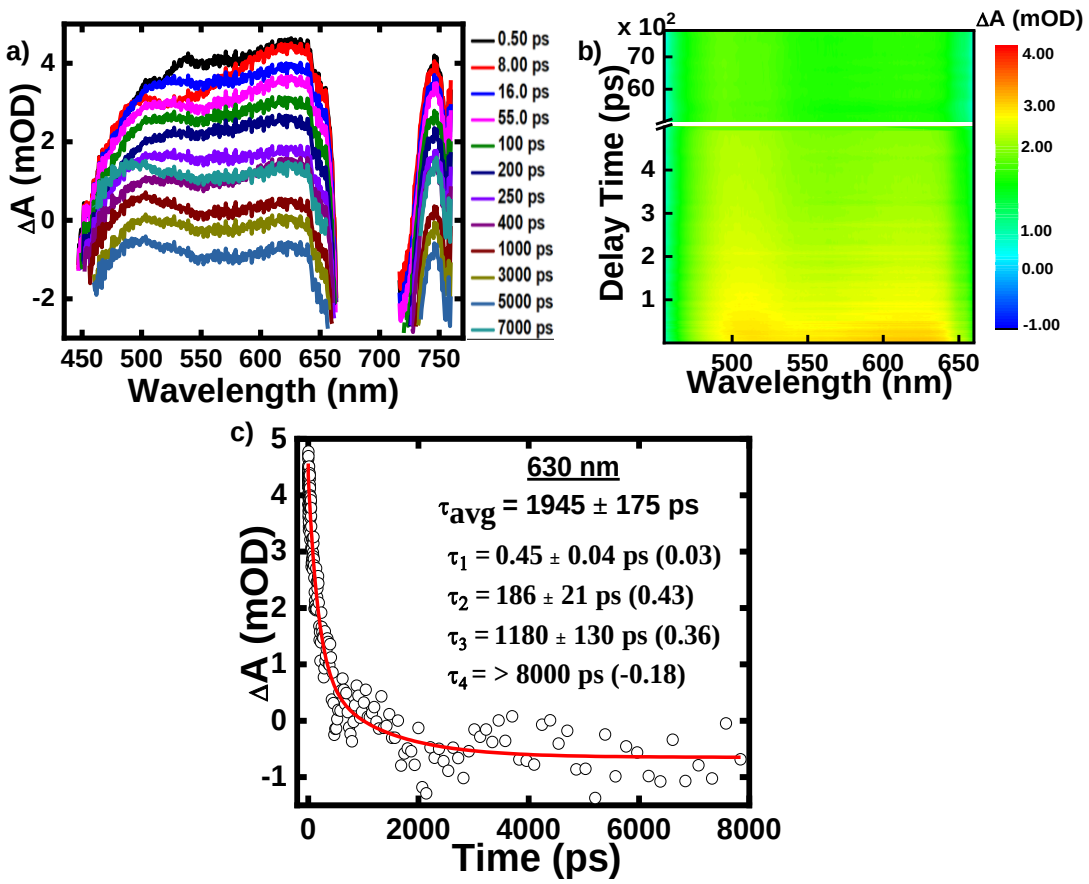

Figure S14. a) Time-dependent fs-TAS profile; b) 2D mapped contour fs-TAS spectra; c) Kinetic decay fitting plot under oxygen in the presence of sodium azide as a singlet oxygen scavenger for **Pyrene-BINOL-4**

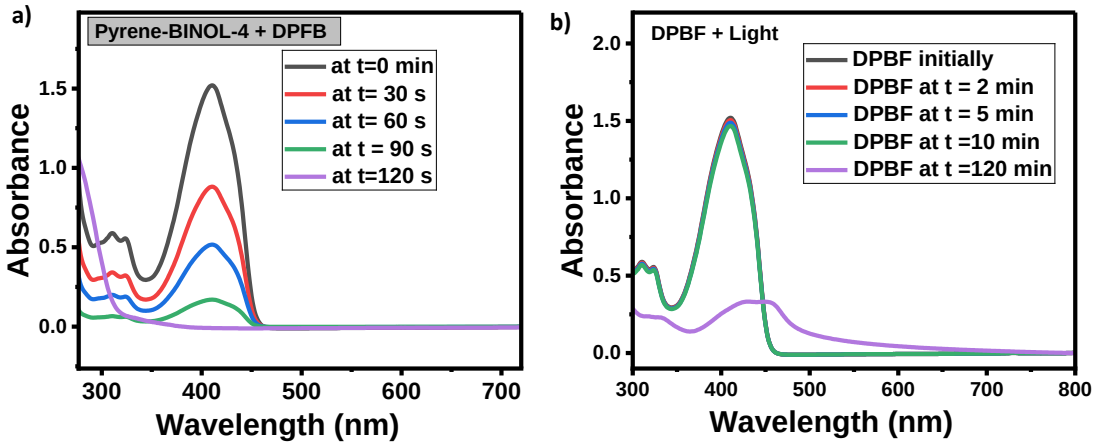

Figure S15. a) Quenching of characteristic peak for DPBF (25 µM) in acetonitrile in the presence of **Pyrene-BINOL-4;** b) The photobleaching experiment of DPBF as a control run (in absence of photocatalyst)

Table S2. Comparison of photocatalytic H_2O_2 production rate of **Pyrene-BINOL-4** with previously reported photocatalysts under sacrificial agent free condition.

Entry	Photocatalyst	Irradiation condition	H_2O_2 production rate ($\mu mol.g^{-1}.h^{-1}$)	Reference
1	RF523	λ > 420 nm 140.3 W m^{-2}	75	*Nat. Mater.* 2019, **18**, 985-993
2	ZnPPc-NBCN	AM 1.5G 100 mW/cm^2	114	*Proc. Natl. Acad. Sci. U. S. A.* 2021**, 118** , e2103964118
3	CdS/PDA	λ = 420 nm, 300 W Xe lamp	3.84 mM in 24 h	*ACS Catal.* 2022, **12**, 11436-11443
4	PEI/g-C3N4	visible light 420 < λ < 800 nm; 300 W xenon lamp	200 μM under 1 h	*ACS Sustain. Chem. Eng.* 2021, **9**, 4520-4530
5	CoOx-NvCN	λ = 420 nm 300 W Xe lamp	244.8 μmol L^{-1} h^{-1}	*ACS Catal.* 2024, **14**, 10893-10903
6	PAF 371	λ > 420 nm, 300 W Xe lamp	923	*ChemCatChem* 2025, **17**, e202401141.
7	SonoCOF-F2	λ > 420 nm, 300 W Xe lamp	275.2 μmol in 96 h	*J. Am. Chem. Soc.* 2022, **144**, 9902-9909
8	RF-DHAQ-2	λ > 420 nm, 300 W Xe lamp	1.82 mmol g^{-1} h^{-1}	*Angew. Chem. Int. Ed.* 2023, **135**, e202218318
9	HEP-TAPT-COF	λ = 420 nm, 300 W Xe lamp	87.50 μmol h^{-1}	*Angew. Chem. Int. Ed.* 2023, **62**, e202217479
10	Ace-asy-CTF	λ = 420 nm, 300 W xenon arc lamp	2594 μmol g^{-1} h^{-1}	*ACS Catal.* 2024, **14**, 17654-17663
11	USTB-10	$\lambda \geq$420 nm	2274 μmol g^{-1} h^{-1}	*Adv. Funct. Mater.* 2022, **32**, 2207394
12	DMCR-1NH	λ = 420 nm 300 W Xe lamp	2264.5 μmol g^{-1} h^{-1}	*J. Am. Chem. Soc.* 2023, **145**, 2975-2984
13	N_0-COF	λ = 495 nm 300 W Xe lamp	1570	*Environ. Sci. Nano.* 2022, **9**, 2464-2469.
14	TpDZ	λ> 420 nm 300 W Xe lamp	7327	*Angew. Chem. Int. Ed.* 2023, **62**, e202310556.
15	FS-COFs	λ> 420 nm 300 W Xe lamp	3904	*Angew. Chem. Int. Ed.* 2023, **62**, e202305355.
16	Bpt-CTF	AM 1.5G 100 mW.cm-^{2}	3268	*Adv. Mater.* 2022, **34,** 2110266
17	MRF-250	λ> 420 nm 300 W Xe lamp	582	*Nano Res.* 2021, **14**, 3267-3273.
18	AQTEE-COP	λ> 400 nm 300 W Xe lamp	3204	*ACS Catal.* 2022, **12**, 12954-12963.
19	**Pyrene-BINOL-4**	**AM 1.5G 100 mW.cm^{-2}**	**3821**	**This work**

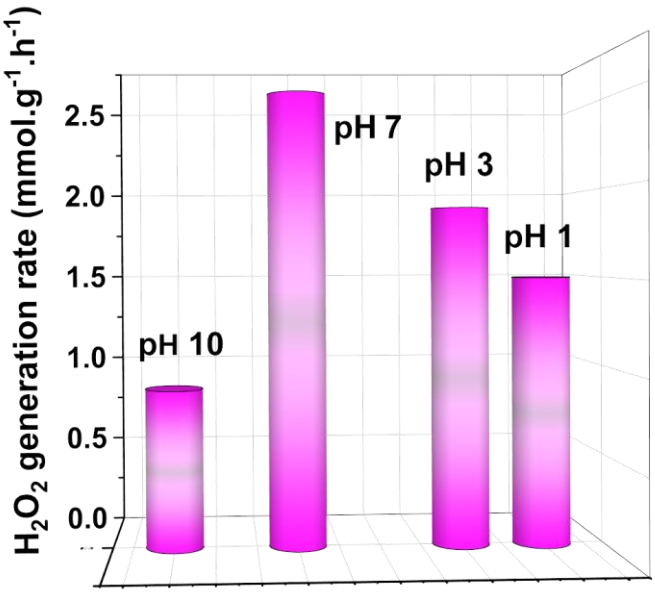

Figure S16. pH-dependent H_2O_2 production of **Pyrene-BINOL-4** from bare water under 50W blue LED.

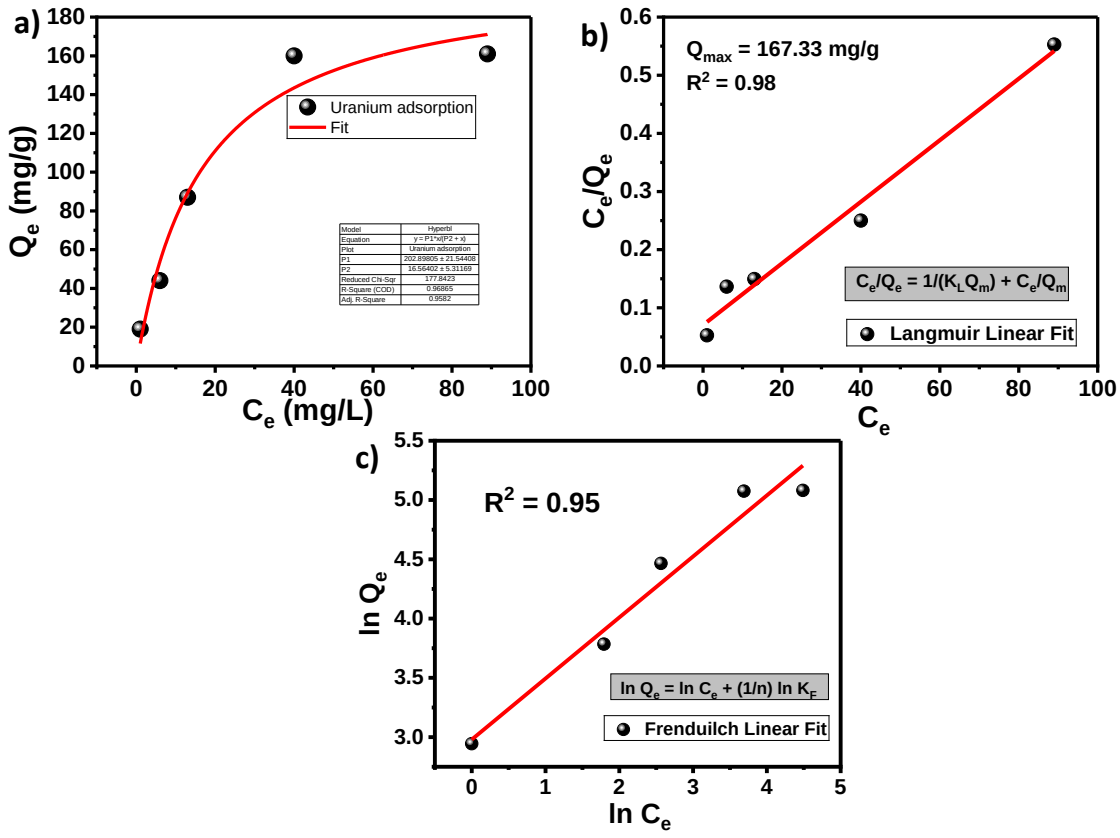

Figure S17. a) Adsorption isotherm for uranium (VI); b) Langmuir model fitting; c) Freundlich model fitting with **Pyrene-BINOL-4**

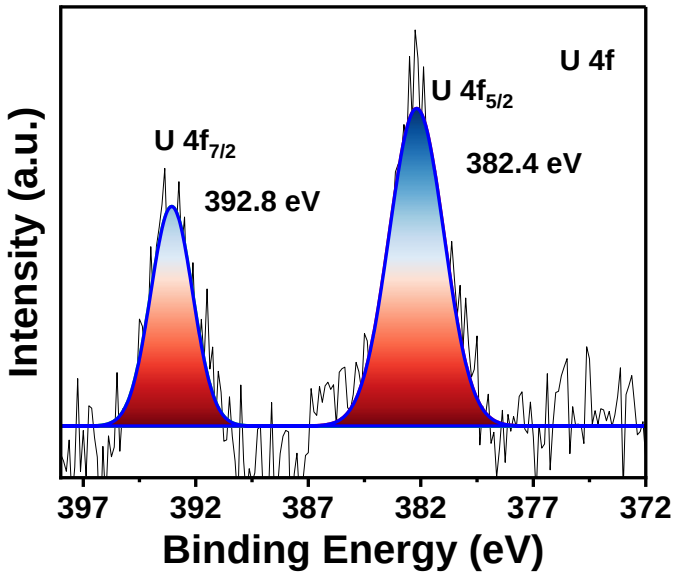

Figure S18. Deconvoluted XPS profile for Uranium 4f after adsorption over **Pyrene-BINOL-4**.

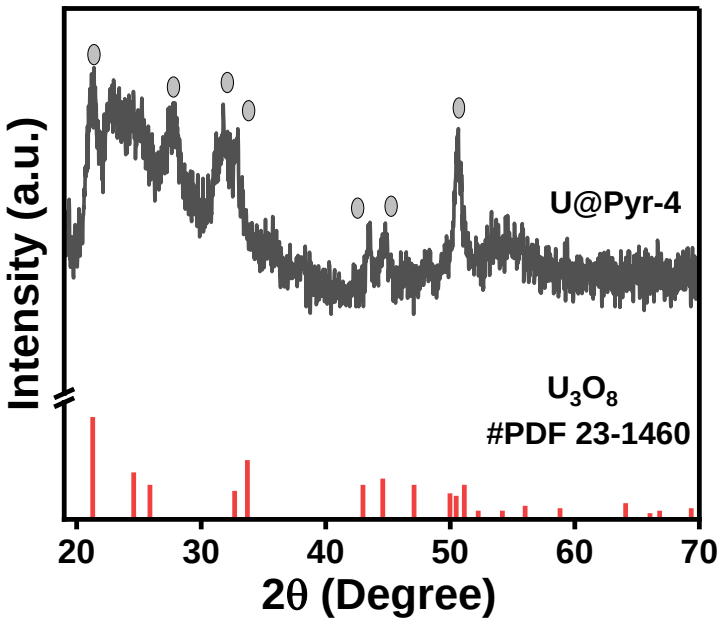

Figure S19. PXRD pattern for **U@Pyr-4** along with the standard PDF card for U_3O_8.

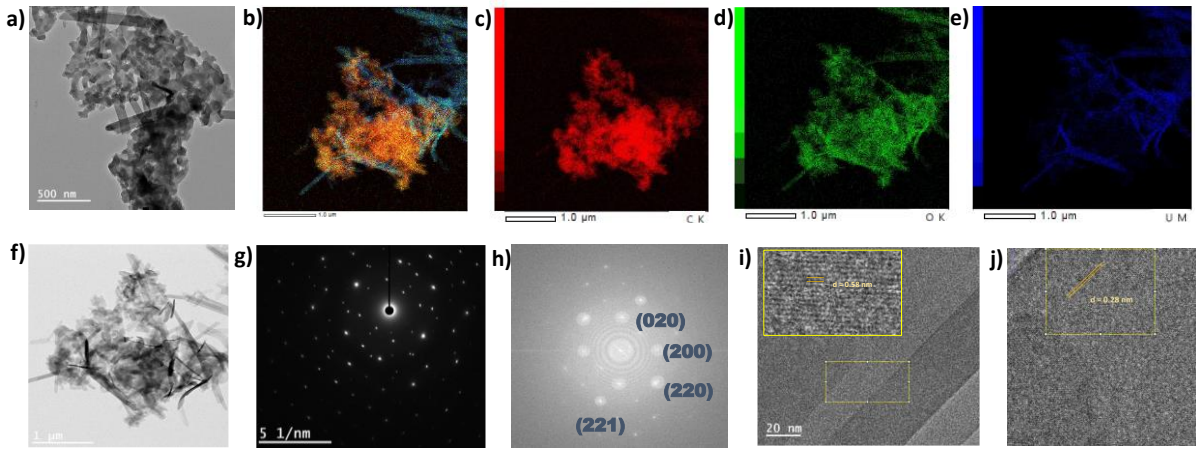

Figure S20. a) HRTEM image; b-e) elemental mapping; f) HRTEM image showing uranium dense region as black; g-h) SAED pattern, and i-j) crystalline fringes for **U@Pyr-4**

U 367.007 {92} (Axial)	
Concentration average	**0.044 ppm**
Concentration per Run 1	**0.043 ppm**
Concentration per Run 2	**0.044 ppm**
Concentration per Run 3	**0.046 ppm**
Concentration RSD	**3.7%**

Figure S21. ICP-OES profile of **U@Pyr-4**.

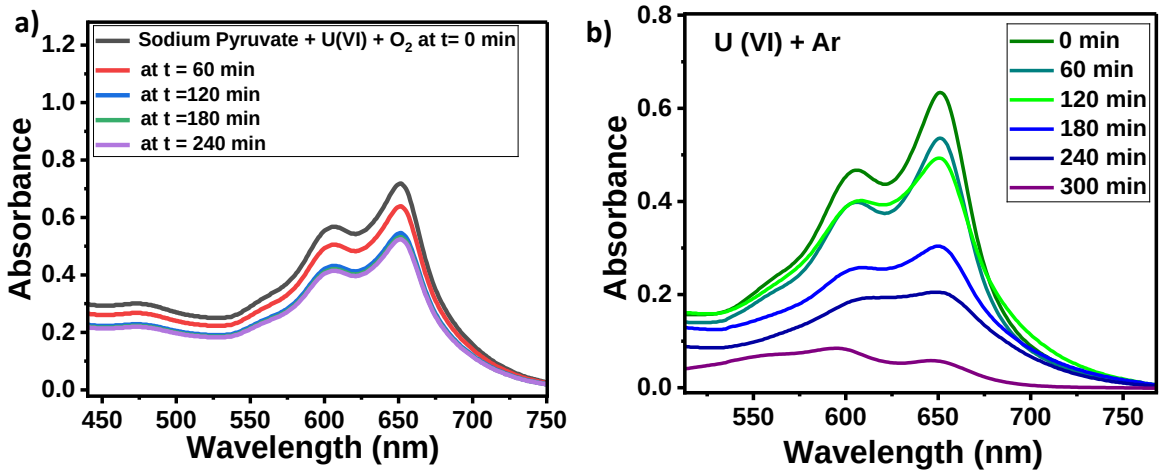

Figure S22. Time-dependent photoimmobilization of uranium(VI) using **Pyrene-BINOL-4** under a) oxygen atmosphere with sodium pyruvate and b) under argon atmosphere.

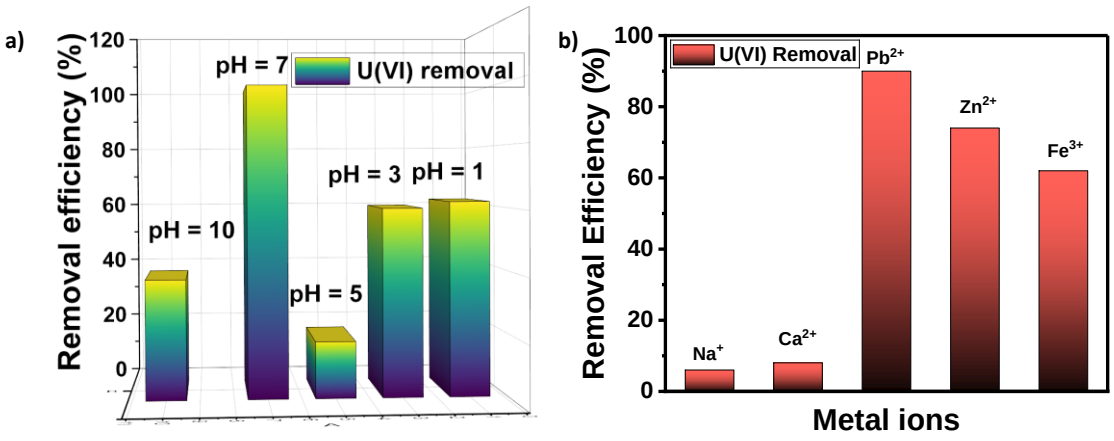

Figure S23. a) Effect of pH and b) effect of different metal ions on uranium photoreduction for **Pyrene-BINOL-4**.

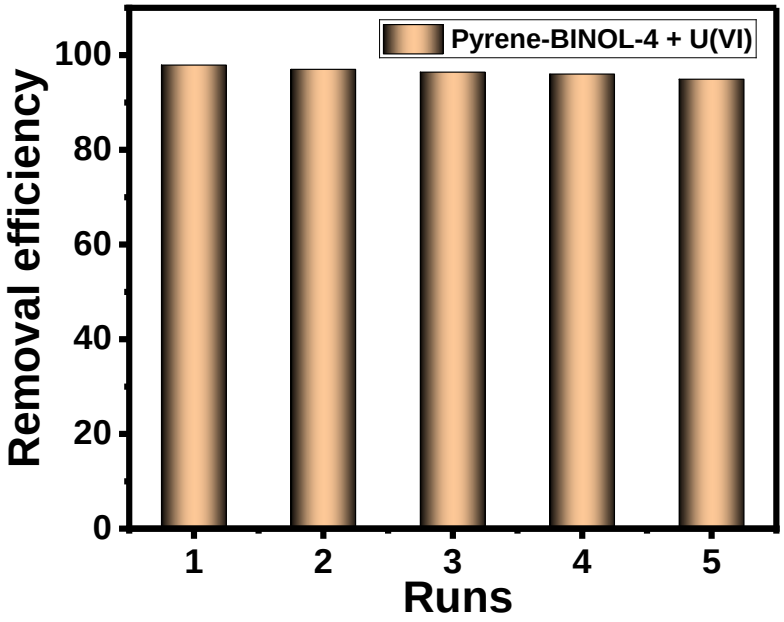

Figure S24. Recycling Experiments for uranium photoremoval with **Pyrene-BINOL-4.**

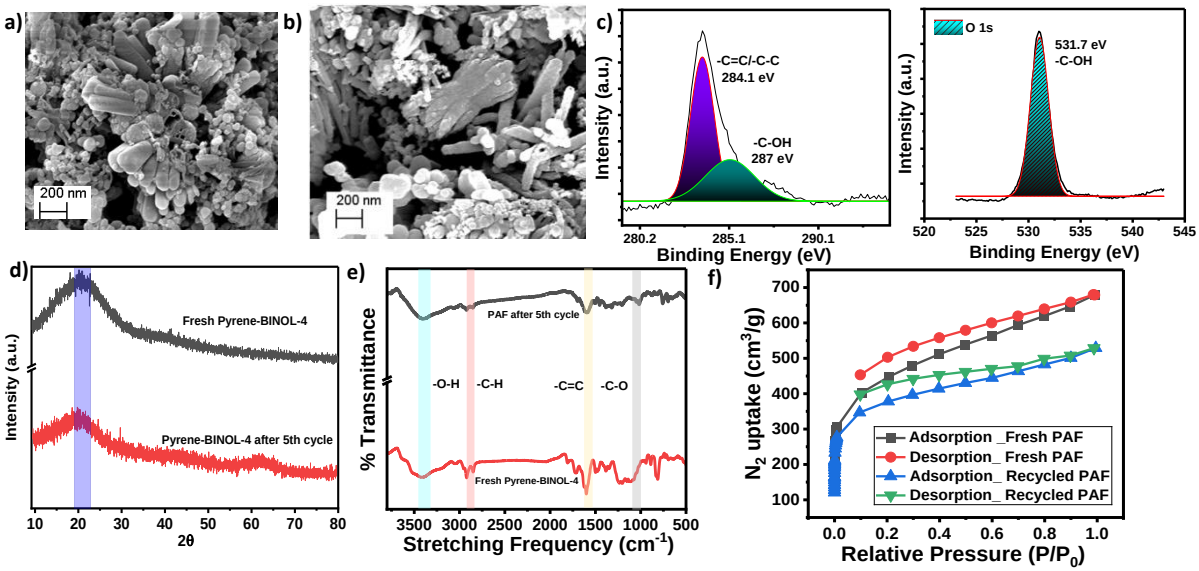

Figure S25. Recyclability test for **Pyrene-BINOL-4** with FESEM a) PAF after 5th cycle; b) Fresh PAF; c) C 1s and O 1s XPS of the recycled PAF; d) PXRD pattern; e) FT-IR spectra; f) BET isotherm after uranium photoimmobilization.

References.

(S1). Gaussian 16, Revision C.01, M. J. Frisch, G. W. Trucks, H. B. Schlegel, G. E. Scuseria, M. A. Robb, J. R. Cheeseman, G. Scalmani, V. Barone, G. A. Petersson, H. Nakatsuji, X. Li, M. Caricato, A. V. Marenich, J. Bloino, B. G. Janesko, R. Gomperts, B. Mennucci, H. P. Hratchian, J. V. Ortiz, A. F. Izmaylov, J. L. Sonnenberg, D. Williams-Young, F. Ding, F. Lipparini, F. Egidi, J. Goings, B. Peng, A. Petrone, T. Henderson, D. Ranasinghe, V. G. Zakrzewski, J. Gao, N. Rega, G. Zheng, W. Liang, M. Hada, M. Ehara, K. Toyota, R. Fukuda, J. Hasegawa, M. Ishida, T. Nakajima, Y. Honda, O. Kitao, H. Nakai, T. Vreven, K. Throssell, J. A. Montgomery, Jr., J. E. Peralta, F. Ogliaro, M. J. Bearpark, J. J. Heyd, E. N. Brothers, K. N. Kudin, V. N. Staroverov, T. A. Keith, R. Kobayashi, J. Normand, K. Raghavachari, A. P. Rendell, J. C. Burant, S. S. Iyengar, J. Tomasi, M. Cossi, J. M. Millam, M. Klene, C. Adamo, R. Cammi, J. W. Ochterski, R. L. Martin, K. Morokuma, O. Farkas, J. B. Foresman, D. J. Fox, Gaussian, Inc., Wallingford CT, **2016**.

(S2). A. D. Becke, *J. Chem. Phys.***1993**, *98*, 5648-5652.

(S3) C. Lee, W. Yang, R.G. Parr, *Phys. Rev. B* **1988**, *37*, 785– 789.

(S4). T. Yanai, D. P. Tew, N. C. Handy, *Chem. Phys. Lett.* **2004**, *393*(1–3), 51.

(S5). S. Grimme, J. Antony, S. Ehrlich, H. A. Krieg, *J. Chem. Phys.*, **2010**, *132*,154104–154119.

(S6). A. V. Marenich, C. J. Cramer, D. G. Truhlar, *J. Phys. Chem. B.*, **2009**, *113*, 6378– 639.

(S7). Jr. J. Wyman, *J. Am. Chem. Soc.* **1936**, *58*, 1482−1486

(S8). D. E. Glendening, A. E. Reed, J. E. Carpenter and F. Weinhold, NBO, version 3.1.; University of Wisconsin: Madison, WI, **1993.**